Aalto University

OPEN ACCESS

This is an electronic reprint of the original article.
This reprint may differ from the original in pagination and typographic detail.

Malan, Willem Dutoit; Akdogan, Guven; Taskinen, Pekka; Hamuyuni, Joseph; Zietsman, Johan

Phase equilibria and thermodynamic evaluation of the Ti-V-O system in air

Published in:
Calphad: Computer Coupling of Phase Diagrams and Thermochemistry

DOI:
10.1016/j.calphad.2018.10.006

Published: 01/12/2018

Document Version
Peer-reviewed accepted author manuscript, also known as Final accepted manuscript or Post-print

Published under the following license:
CC BY-NC-ND

Please cite the original version:
Malan, W. D., Akdogan, G., Taskinen, P., Hamuyuni, J., & Zietsman, J. (2018). Phase equilibria and thermodynamic evaluation of the Ti-V-O system in air. *Calphad: Computer Coupling of Phase Diagrams and Thermochemistry*, *63*, 220-228. https://doi.org/10.1016/j.calphad.2018.10.006

This material is protected by copyright and other intellectual property rights, and duplication or sale of all or part of any of the repository collections is not permitted, except that material may be duplicated by you for your research use or educational purposes in electronic or print form. You must obtain permission for any other use. Electronic or print copies may not be offered, whether for sale or otherwise to anyone who is not an authorised user.

Phase equilibria and thermodynamic evaluation of the Ti-V-O system in air

Willem Dutoit Malan[a], Guven Akdogan[b], Pekka Taskinen[c], Joseph Hamuyuni[c], Johan Zietsman[a]

[a]*Department of Material Sciences and Metallurgical Engineering, University of Pretoria, Private Bag X20, Hatfield, 0028, South Africa*
[b]*Department of Process Engineering, Stellenbosch University, Banghoek Rd, 7599, South Africa*
[c]*Metallurgical Thermodynamics and Modelling, School of Chemical Engineering, Aalto Unviersity Vuorimiehentie 2K, FI-00076 Aalto*

Abstract

The Ti-V-O system was studied experimentally from 700 °C to 1500 °C by high-temperature equilibration, quenching, scanning electron microscope and Energy-Dispersive X-Ray spectroscopy. The solubility of titanium in the slag is less than 3 mole % at 1500 °C and the vanadium solubility in the rutile phase reached a maximum of 7.8 mole % at 1400 °C. The thermodynamic evaluation was performed with FactSage 7.0. The solubility of vanadium in the rutile phase was developed within the framework of the compound energy formalism. The properties of the liquid phase were described with the quasichemical model. A set of self-consistent thermodynamic parameters was estimated well within acceptable limits. The calculated phase diagram of the Ti-V-O system in air is presented and compared to experimental observations and other phase diagram data from literature.

Key words: Ti-V-O system, thermodynamics, static experiments, phase diagram

1. Introduction

In an earlier study [1] the Fe-V-O system in air was investigated and its industrial importance, particularly in the extraction of vanadium from titaniaferous magnetite was explained. In this study, we investigate the Ti-V-O system in air, which in turn will contribute to thermochemical database for M-V-O systems (where M refers to metallic elements like Na, K, Ca, Mg, Ti, Cr, Mn, Fe, Al, and Si) under oxidizing conditions. Only a few studies have partially investigated phase equilibria of Ti-V-O in air and at lower oxygen partial pressures [2, 3, 4, 5]. Nevertheless, the Ti-V-O system was thermodynamically evaluated by Enomoto [6] and later again by Yang et al. [7] in response to new experimental phase diagram data obtained under relatively reducing conditions [4, 5, 8].

Applications of the Ti−V−O system under oxidizing conditions were reported by numerous studies [9, 10, 4, 5]. One such application of the Ti-V-O system under oxidizing conditions is its effect as supportive promoter for catalyst during the selective oxidation of butadiene, 1-butene, and benzene to maleic anhydride, and of naphtalene and o-oxylene to phthalic anhydride [9]. A better knowledge of phase relations assists in identifying appropriate processing conditions and to understand the ageing phenomena of catalysts [4].

Phase equilibrium data for Ti-V-O system in equilibrium with air is scarce at temperatures below 800 °C and non-existent above 800 °C. For this reason, this study focusses on characterization of liquidus and solidus composition from 700 °C to 1500 °C by means of equilibration-quench-analysis method. The solubility of V in the rutile phase is estimated and solid state equilibria of stoichiometric compounds are investigated. Furthermore, the system is critically evaluated and thermodynamically assessed with the well-known CALPHAD (Calculation of Phase Diagrams) method. All calculations were performed with the commercial software package, FactSage 7.0 [11]. This study is part of a larger effort to measure and model the thermochemical behaviour of vanadium-containing oxide systems.

2. Literature Data

2.1. Structure and phase transformation data

Fotiev et al. [3] studied compatibility relations among crystalline phases of the oxide components Fe_2O_3, TiO_2, and V_2O_5 in air employing a quenching technique. A solid-phase compatibility triangle applicable to restricted temperature ranges below 700 °C, for the pseudo-ternary system $Fe_2O_3-TiO_2-V_2O_5$ is presented in their study. No

stoichiometric compounds were found in the $TiO_2-V_2O_5$ phase region, and no ternary stoichiometric compounds were reported. In the same study, compatibility relations among crystalline phases of the pseudo-ternary systems, $Al_2O_3-TiO_2-V_2O_5$ and $Cr_2O_3-TiO_2-V_2O_5$ were investigated. An identical experimental method was employed as for the pseudo-ternary system, $Fe_2O_3-TiO_2-V_2O_5$. The presented $Al_2O_3-TiO_2-V_2O_5$ and $Cr_2O_3-TiO_2-V_2O_5$ pseudo-ternary phase diagrams give solid-phase compatibility triangles applicable to temperatures below 900 °C. No binary or ternary compounds were reported in these systems.

In another study, Golovkin et al. [12] investigated sub-solidus regions in the $Cr_2O_3-TiO_2-V_2O_5$ system. Samples were equilibrated at 700 °C with repeated re-grounding and pellitizing cycles. No stoichiometric compounds were found in the $TiO_2-V_2O_5$ pseudo-binary system.

Five low-temperature, low-pressure polymorphs of TiO_2 have been reported [13, 14, 15]. However, only anatase and rutile are found in the FToxid database of FactSage thermochemistry software. The transition of anatase to rutile is a nucleation and growth process and has been shown in most cases to transform between 600 and 700 °C. The transition temperature is dependent on particle size, particle shape, surface area, atmosphere, volume of sample, nature of sample container, heating rate, soaking rate, impurities and measurement technique [16].

Habel et al. [4] investigated the transformation from anatase to rutile in the presence V_2O_5 and reported a transformation temperature of 550 °C. This finding suggested that V_2O_5 encouraged the transformation of rutile to anatase. This experimental observation supports our experimental assumption that anatase in the presence V_2O_5 was transformed to rutile, given that all experiments of this study were conducted at and above 700 °C with relatively long equilibration times. Moreover, it has been reported that rutile has a deviation from stoichiometry corresponding to oxygen deficiency (see subsection 4.4).

The structure of V_2O_5 is orthorhombic based on the hcp oxygen packing scheme. The compound has been well described in numerous studies [17, 18, 19, 20].

2.2. Liquidus and solidus data

Little liquidus and solidus data have been reported for the Ti-V-O system in air (see Table 1). However, in two recent studies by Habel et al. [4, 5] a wide solubility range of V_2O_5 in rutile crystal structure was reported. The focus of their work was on phase development during catalyst processing under oxidizing conditions. A phase field for rutile solid solution up to 12.5 mole % V_2O_5 at 675 °C was detected and a eutectic reaction from cooling was found at 631 °C by means of DTA (differential thermal analysis). However, it was found that the thermal arrest upon heating was estimated to be about 670 °C. It is stated in Yang et al. [7] that it is more appropriate to assign the heating value than the cooling value to the eutectic temperature, given that there is a likelihood of potential supercooling during solidification. A preliminary phase diagram displaying a large solubility area of V_2O_5 in rutile was deduced from a set of XRD (X-ray diffraction) results.

It was then reported that the unit cell of rutile solid solution is smaller than that of pure rutile, because V^{5+} and V^{4+} ions are smaller than Ti ions. This type of behaviour indicates a substitutional replacement. A set of different defect models was proposed, describing V_2O_5(s) solubility in the rutile phase [4].

- Vanadium remains completely in a 5+ valance state, which indicates that no oxygen was lost and charge compensation on the crystal lattice of rutile is preserved by interstitial oxygen ions:

$$V_2O_5 \Rightarrow 2V_{Ti} + O_i'' + 4O_o^x \tag{1}$$

- Vanadium remains entirely in a 5+ valance state, which indicates that no oxygen was lost and charge compensation on the crystal lattice of rutile is preserved by vacancies on the vanadium site:

$$2V_2O_5 \Rightarrow 4V_{Ti} + Va_{Ti}'''' + 10O_o^x \tag{2}$$

- Vanadium is reduced to a a 4+ valance state with a loss of $1/2O_2$

$$2V_2O_5 \Rightarrow 2V_{Ti}^x + 4O_o^x + 1/2O_2(v)\uparrow \tag{3}$$

Table 1: Invariant reactions and phase transitions in the Ti−V−O system in air from literature.

Method	Composition (V_2O_5 mole %)	Temperature °C	Type of invariant	Equilibrium solid phases	Reference
DTA	95	670	Eutectic	V_2O_5, TiO_2	[4]
Thermodynamic assessment	95	675	Eutectic	V_2O_5, TiO_2	[7]

The last defect reaction is unlikely to take place, because of oxidizing conditions during experimentation. XPS (X-ray photoelectron spectroscopy) studies from Habel et al. [4] revealed an oxidation state of 4.75 for V in the rutile phase. As a result, the first and second defect models are used for deriving a set of mathematical equations for describing the solid solution between TiO_2(s) and V_2O_5(s).

It is mentioned in section 1 that the Ti-V-O system has been assessed and optimized by Yang et al. [7]. Yang et al. [7] used the the ionic liquid model to describe the liquid phase and all solid phases were developed within the framework of the compound energy formula. All available experimental data pertaining to the Ti-V-O system were critically evaluated and a set of self-consistent thermodynamic model parameters was obtained. However, limited experimental data on the $TiO_2-V_2O_5$ phase region were obtained and the phase diagram presented by Yang et al. [7] was based exclusively on data from Habel et al. [4]. As a result, the authors relied on extrapolation from model parameters to calculate the higher temperature areas of the liquidus and solidus on the V_2O_5-TiO_2 phase diagram. Because of the lack of experimental data, it was stated by Yang et al. [7] that "it is important to note that more reliable experimental investigations are necessary to further improve the description of this system".

2.3. Thermodynamic data

All thermodynamic data of V_2O_5(s,l) and TiO_2(s,l) were taken from FactPS database [11], unless otherwise stated (see Table 2). No other thermodynamic data of the Ti-V-O system in air were found in literature, which highlights the need for further experimental work.

Table 2: Calculated enthalpies and entropies of pure compounds in the Ti-V-O system compared with the experimental data.

Compound	$\Delta H^\circ_{f,298}$ J.mol^{-1}	S°_{298} Jmol^{-1}K^{-1}	a	b	c	d	e	f	C_p range K	Reference
Solids										
TiO_2(s)	-944750.00	50.460	77.848				- 33.67841	40.2940672	298- 2130	[11]
V_2O_5(s)	-1550590	130.559	25.970	50.00	5853.80	-76.76761	-7.541627		298- 943	[11]
Liquid										
V_2O_5(l)	-1491202	191.96	164.31	24.00			-36.28207		298 - 600	[11]
TiO_2(l)	-898726.0	72.068	77.840				- 33.67841	40.2940672	298- 2130	[11]
Ti_2O_3(l)	-1414375	130.17	169.96		-750.22		16.09649	-15.6552100	298 - 2115	[11]

$$Cp(Jmol^{-1}K^{-1}) = a + b(10^{-3})T + cT^{-0.5} + d(10^3)T^{-1} + e(10^5)T^{-2} + f(10^7)T^{-3}$$

3. Experiments

3.1. Sample Preparation

High-purity V_2O_5(s) and TiO_2(s) were selected as starting materials. The material, source and purity are given in Table 3. Mixtures of selected bulk compositions of less than 0.5 g were prepared by weighing the oxide powders, followed by grinding a mixture thoroughly in an agate mortar. The initial composition was selected to insure that a liquid phase is in equilibrium with a solid phase at a desired temperature. The sample was then pelletized to a diameter of 8 mm and a height of more or less 3 mm in a pressing tool.

3.2. Experimental Procedure

Equilibration was accomplished in a vertical electrical resistance tube furnace (Lenton, UK) with a 35 mm inner diameter alumina work tube. Before any tests were conducted, the hot zone of the furnace was determined by obtaining a thermal profile at 700 °C, 1000 °C and 1300 °C. A calibrated S-Type thermocouple connected to a Keithley

Table 3: Purity of initial materials and sources they were acquired from.

Material	Source	Purity
Divanadium Pentaoxide	SIGMA ALDRICH, RSA	99.60%
Titanium dioxide (Anatase)	SIGMA ALDRICH, RSA	>99 %

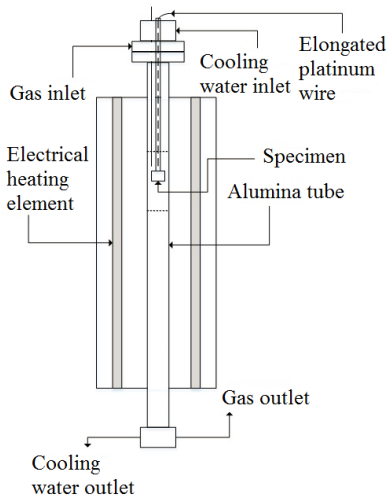

(a) Schematic of the vertical front view section of the furnace and auxiliaries

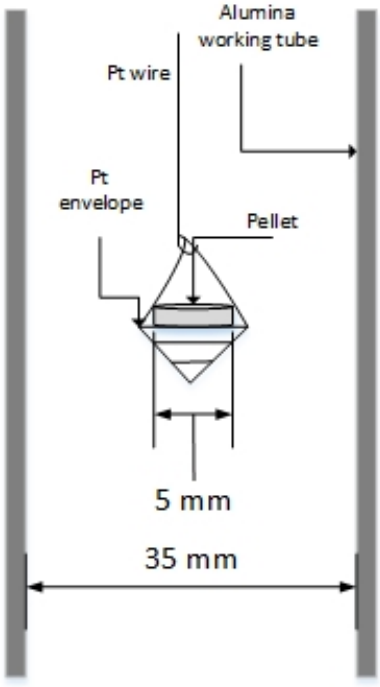

(b) Envelope design and suspension of the pellet in the furnace

Figure 1: Furnace and suspension design

2010 DMM multimeter (Cleveland, OH, USA), and a cold junction compensation was connected to a Keithley 2000 multi-meter (Cleveland, OH, USA) to measure the ambient temperature with a PT100 sensor (Platinum Resistance thermometer, SKS Group, Finland). The temperature was captured and logged every 2 seconds with a NI labVIEW temperature logging program. A small hot zone of 4 - 5 cm in length was established. The deviation of temperature measurements in the hot zone was less then 2 °C. The hot zone is shown in Figure 1a as an area within the two dashed lines.

Experiments were carried out in air, with the top and bottom of the furnace open to the atmosphere. All specimens were lowered into the furnace with Pt wire in a Pt envelope. The advantages of using platinum as containing material are:

- The Pt wire and envelope will not react with oxygen to then dissolve in the oxide phases of a specimen.
- Pt melts at 1770 °C, which is well above the desired temperature range of this study.
- A hand assembled envelope with small voids was chosen over Pt foil to allow the specimen to come in direct contact with the quenching medium.

Equilibrium was confirmed by two means: Comparing samples from different equilibration times to each other and assessment of compositional homogeneity of the phases by Scanning electron microscope with energy dispersive

X-Ray spectroscopy (SEM-EDS) and Electron probe micro-analysis (EPMA). Careful consideration was given to equilibration times. For samples equilibrated at and below 800 °C, equilibrium was achieved after 32 hours. For samples above 800 °C and below 1200 °C, equilibrium was achieved after 16 hours. And for samples at and above 1200 °C, equilibrium was achieved after 4 hours. Each experiment was repeated at least once.

The equilibration time was mainly dependent on temperature, because of the influence of temperature on diffusion, phase transitions and chemical reactions. Physical properties of a material, such as solid-liquid surface tension, liquid viscosity and density are assumed to have a negligible effect on equilibration time compared to temperature. After equilibrium was achieved, a sample was rapidly dropped in a beaker of ice-water. Rapid quenching attempts to preserve the phase assemblage formed at the equilibration temperature. The quenched sample was dried and mounted in a epoxy resin. After solidification, the sample was ground and polished employing conventional metallographic techniques. However, water was not used as lubricant because V_2O_5(s) has a solubility of 0.8 g/l in water [21]. For this reason, propylene glycol (Sigma Aldrich, Germany) and DP Lubricant Brown (Struers, Munich, Denmark) were used.

The polished samples were carbon coated with a Leica EM SCD050 coater (supplied by Leica Mikrosysteme GmbH, Vienna), before Scanning electron microscopy (SEM, A LEO 1450, Carl Zeiss Microscopy GmbH, Jena, Germany) with Energy Dispersive analysis (EDS, Link Inca X-sight 7366, Oxford Instruments plc, Abingdon, Oxfordshire, UK) and EPMA (Cameca SX 100). Carbon coating avoids charge build-up of a specimen, which reduces thermal damaging of samples and improves secondary electron signal thereby improving imaging. The accelerating voltage of the SEM was 15 KV and standard intensities for O, V and Ti were hematite, pure V and Ti, respectively. All EPMA samples were analysed at 15 KV accelerating voltage and 40 nA beam current. All elements were measured on their Kα lines, using wavelength-dispersive spectrometers. Ti was calibrated on TiO_2, V on pure V, but the measured V mass fractions were adjusted as if V had been calibrated on vanadinite ($Pb_5(VO_4)_3Cl$). This was done to better match the matrix of the calibration standard with the oxide matrix of the samples. The matrix correction in the probe software was based on the "X-PHI" model [22].

4. Thermodynamic modelling

4.1. Stoichiometric Compounds

The Gibbs energies of stoichiometric compounds and of the components of solution phases are expressed in the form of $G - \sum H_{SER}$ and is also as a function of temperature. The $\sum H_{SER}$ (Standard Element Reference) is the sum of enthalpies of the elements at 298 K and 1 bar pressure. The standard Gibbs energy of stoichiometric compounds are described by:

$$G^{\circ}(T) = \left(\Delta H_{f,298K} + \int_{298K}^{T} C_p(T)dT\right) - T\left(S^{\circ}_{298K} + \int_{298K}^{T}(C_p(T)/T)dT\right) \tag{4}$$

where the parameters of some compounds from Equation 4 are optimized from selected literature data reviewed in section Literature Data. In this case, only the enthalpy of formation and standard entropy of some compounds were optimized to reproduce the experimental observations from this study.

4.2. Gas Phase

All thermodynamic calculations were done at an absolute pressure of 1 atm. At this low pressure the gas phase exhibits ideal gas behaviour. The following limiting condition supports the assumption [23]:

$$\lim_{P\to 0}\frac{f_i}{p_i} \equiv 1 \tag{5}$$

Moreover, the molar Gibbs energy of the gas phase is given as [23]:

$$G_m = \sum_i x_i G_i^{\circ} + RT\sum_i x_i ln x_i + RT ln(P_i/P_{\circ}) \tag{6}$$

where x_i is the mole fraction of the specie i, $P_{\circ}$ is the standard pressure of 1 atm and P_i is the partial pressure of the gaseous specie, i.

4.3. Modelling of the liquid phase

The modified quasichemical model (MQM) [24, 25], which takes into account short range ordering of second nearest neighbours was used to describe the liquid phase. At least one set of cation pairs need to be identified when MQM is used in order to present a quasichemical reaction.

In the Ti-V-O slag it is assumed that V_2O_5(l) consists of the building unit $V_2O_7^{4-}$, which corresponds to $V_2O_3^{4+}$ cation specie. Adopting such a building unit of liquid V_2O_5 was supported experimentally by Kawakita et al. [26] and Hawakawa and Yoko [27] who had investigated the local structures of liquid and vitreous V_2O_5 and P_2O_5 melts [26, 27]. Moreover, Hudon and Jung [28] and Rahman et al. [29] successfully adopted $P_2O_7^{4-}$ as building unit of P_2O_5 in the $CaO-P_2O_5$ and $SiO_2-P_2O_5$ systems. This approach has also been adopted by FactSage for describing slag phases containing P_2O_5 [30]. Kawakita et al. [26] had shown that he characteristics of liquid P_2O_5 is similar to liquid V_2O_5, which further supports our usage of $V_2O_7^{4-}$ as building unit of V_2O_5(l). Furthermore, the liquid phase will likely contain a low concentration of V^{4+} ions. This is because of the equilibrium reaction $V_2O_5(l) = 2VO_2(l) + 1/2O_2(g)$ [31], which has been shown to become thermodynamically favourable in air at just below 1400 °C [11]. However, no study has shown experimentally whether TiO_2(l) stabilize or destabilize the higher valence V^{5+} ions, hence it is assumed that the V_2O_5 liquid component is largely dominant and the species with lower oxidation states in air were excluded. This assumption was also made by Xie et al. [32], Malan et al. [1], Cao et al. [33].

The quasichemical reaction between cations in a slag phase of the Ti-V-O in air can be expressed as:

$$(\mathrm{Ti}^{4+} - \mathrm{Ti}^{4+}) + (\mathrm{V_2O_3^{4+}} - \mathrm{V_2O_3^{4+}}) = 2(\mathrm{Ti}^{4+} - \mathrm{V_2O_3^{4+}}) \qquad \Delta g_{\mathrm{Ti}^{4+}-\mathrm{V_2O_3^{4+}}} \tag{7}$$

where $\Delta g_{\mathrm{Ti}^{4+}-\mathrm{V_2O_3^{4+}}}$ represents the Gibbs energy change of the quasichemical reaction 7. However, Ti has multiple oxidisation states, and is it known that Ti^{3+} is present in low concentrations under oxidizing conditions, because of the decomposition of TiO_2(l) to form Ti_2O_3(l) and O_2(g) in high temperature regions [11]. Therefore, two more quasichemical reactions are identified.

$$(\mathrm{Ti}^{3+} - \mathrm{Ti}^{3+}) + (\mathrm{V_2O_3^{4+}} - \mathrm{V_2O_3^{4+}}) = 2(\mathrm{Ti}^{3+} - \mathrm{V_2O_3^{4+}}) \qquad \Delta g_{\mathrm{Ti}^{3+}-\mathrm{V_2O_3^{4+}}} \tag{8}$$

$$(\mathrm{Ti}^{4+} - \mathrm{Ti}^{4+}) + (\mathrm{Ti}^{3+} - \mathrm{Ti}^{3+}) = 2(\mathrm{Ti}^{4+} - \mathrm{Ti}^{3+}) \qquad \Delta g_{\mathrm{Ti}^{4+}-\mathrm{Ti}^{3+}} \tag{9}$$

$Ti^{3+} - V_2O_3^{4+}$ binary pair was assumed to have ideal mixing behaviour, because under oxidizing conditions, Ti^{3+} concentration was assumed to be low in the studied temperature range (700 °C to 1500 °C) compared to $V_2O_3^{4+}$ concentration. Under oxidizing conditions, the $Ti^{3+} - V_2O_3^{4+}$ binary pair might only start contributing to the Gibbs energy of the liquid phase in temperatures above 1500 °C, because of the further decomposition of TiO_2(l) to form Ti_2O_3(l) and O_2(g). The quasichemical model parameters of the $TiO_2-Ti_2O_3$ system were first optimized by Eriksson and Pelton [34] and later again by Kang et al. [35] in response to the publication of more recent experimental data. Hence, the parameters of Kang et al. [35] are used in this study.

The molar Gibbs energy of the respective $TiO_2-V_2O_5$ and $Ti_2O_3-V_2O_5$ solutions are expressed as follows:

$$\mathrm{G_m} = \mathrm{n_{TiO_2}} g^{\circ}_{\mathrm{TiO_2}} + \mathrm{n_{V_2O_5}} g^{\circ}_{\mathrm{V_2O_5}} - \mathrm{T\Delta S^{config}} + \mathrm{n_{Ti^{4+}-V_2O_3^{4+}}} (\Delta g_{\mathrm{Ti^{4+}-V_2O_3^{4+}}}/2) \tag{10}$$

$$\mathrm{G_m} = \mathrm{n_{Ti_2O_3}} g^{\circ}_{\mathrm{Ti_2O_3}} + \mathrm{n_{V_2O_5}} g^{\circ}_{\mathrm{V_2O_5}} - \mathrm{T\Delta S^{config}} + \mathrm{n_{Ti^{3+}-V_2O_3^{4+}}} (\Delta g_{\mathrm{Ti^{3+}-V_2O_3^{4+}}}/2) \tag{11}$$

where, ΔS^{config} is the configuration entropy expressed as random mixing of the bonds over bond sites in one dimension (Ising approximation) [36]. Moreover, $\Delta g_{\mathrm{Ti^{4+}-V_2O_3{}^{4+}}}$, can be expanded as an empirical polynomial function in the mole fractions of pairs.

$$\Delta g_{\mathrm{Ti}^{4+}-\mathrm{V_2O_3^{4+}}} = \Delta g^{\circ}_{\mathrm{Ti}^{4+}-\mathrm{V_2O_3^{4+}}} + \sum_{\mathrm{i}\geq 1} g^{\mathrm{i0}}_{\mathrm{Ti}^{4+}-\mathrm{V_2O_3^{4+}}} \mathrm{X^i_{Ti^{4+}-Ti^{4+}}} + \sum_{\mathrm{j}\geq 1} g^{\mathrm{0j}}_{\mathrm{Ti}^{4+}-\mathrm{V_2O_3^{4+}}} \mathrm{X^j_{V_2O_3^{4+}-V_2O_3^{4+}}} \tag{12}$$

$\Delta g^{\circ}_{\mathrm{Ti}^{4+}-\mathrm{V_2O_3^{4+}}}$, $g^{\mathrm{0j}}_{\mathrm{Ti}^{4+}-\mathrm{V_2O_3^{4+}}}$ and $g^{\mathrm{0j}}_{\mathrm{Ti}^{4+}-\mathrm{V_2O_3^{4+}}}$ are temperature dependent adjustable model parameters and were optimized to express the properties of the liquidus within reasonable uncertainty limits.

The $\Delta g^{\circ}_{Ti^{4+}-V_2O_3^{4+}}$ term becomes significant at composition of maximum short range ordering. It is known that maximum short range ordering usually occurs at the intermediate compound with the highest melting point (congruent melting) and the minimum mixing enthalpy [32, 28, 37, 38]. However, it was supported experimentally that no intermediate compounds exist in the Ti-V-O system in air. Therefore, the term $\Delta g^{\circ}_{Ti^{4+}-V_2O_3^{4+}}$ may have a lesser impact on the Gibbs energy of the liquid phase compared to the terms, $g^{i0}_{Ti^{4+}-V_2O_3^{4+}}$ and $g^{0j}_{Ti^{4+}-V_2O_3^{4+}}$. Furthermore, it is known when the total mole fraction of V_2O_5 is $<< 1/2$, $X_{V_2O_3^{4+}-V_2O_3^{4+}}$ is small and $g^{0j}_{Ti^{4+}-V_2O_3^{4+}} X_{V_2O_3^{4+}-V_2O_3^{4+}}$ will have a small effect on the Gibbs energy of the liquid. In this region, only the parameters $g^{i0}_{Ti^{4+}-V_2O_3^{4+}}$ largely contribute to the Gibbs energy. The opposite is true when the total mole fraction of TiO_2 is $<< 1/2$ [36].

Furthermore, the $TiO_2-Ti_2O_3-V_2O_5$ liquid properties were described from corresponding binary pairs using a Kohler interpolation method. This method is symmetric in nature, which constitutes that all chemical components are chemically similar. This interpolation method is used as first approach in this study to estimate thermodynamic properties and phase diagram data from binary model parameters. It has been shown that a Kohler interpolation method has been successful in describing slag phases of higher order systems [39, 30, 40, 41, 42].

4.4. Modelling Rutile Solid Solution

The rutile solid solutions in the Ti-V-O system in air were developed within the framework of the compound energy formalism (CEF). It is well suited to model solid solutions with two or more distinct sub-lattices. Furthermore, it allows for cations and anions of different valance to mix in different sub-lattices, corresponding to the structure of a solid solution.

$$G_m = \sum_i \sum_j X_i X_j G^{\circ}_{ij} - TS_{config} + G_E \tag{13}$$

X_i and X_j represent the site fractions of constituents i and j on the first and second sub-lattices, respectively. S_{config} is the configurational entropy and is expressed as follows:

$$S_{config} = -R(a\sum_i X_i \ln X_i + b\sum_j X_j \ln X_j) \tag{14}$$

with a and b being the stoichiometric constants of each lattice and R the ideal gas constant.

It was postulated from the thermodynamic assessment of Eriksson and Pelton [34], Kang et al. [35], Cancarevic et al. [15] that rutile or titanium dioxide might exhibit a degree of non-stoichiometry. In other words, the ratio of oxygen to titanium is less than two and the nature of the defect has a structure TiO_{2-x}. Cancarevic et al. [15] discovered some controversy in literature, meaning that experimental data signified either the existence of double oxygen vacancies and free electrons or their combination with interstitially dissolved Ti^{3+} ions. In their work, the oxygen vacancy model was preferred. The reason for this is that the lack of negative charge in the anion sub-lattice due to oxygen vacancies, is effectively compensated by an inclusion of Ti^{3+} cations on the cation sub-lattice. The non-stoichiometry of rutile was described and developed within the framework of the CEF. Rutile was expressed as $(Ti^{4+}, Ti^{3+})(O, Va)_2$. Moreover, Eriksson and Pelton [34] and Kang et al. [35] used a simple Henrian solution of $TiO_{1.5}$ in TiO_2 to describe non-stoichiometry of rutile. This approach is also used in the FactSage thermochemical software.

To account for V solubility in the rutile structure, V can be introduced substitutionally with interstitially dissolved oxygen (first defect model proposed by Habel et al. [4]). If it is assumed that O dissolves interstitially, the rutile structure is extended and expressed as $(Ti^{4+}, Ti^{3+}, V^{5+})(O^{2-}, Va)(O^{2-}, Va)_2$. Vacancies are introduced into both O sub-lattices for charge neutrality. The extended rutile structure has twelve end-member species, compared to four end-member species when non-stoichiometry is not considered with the introduction of Ti^{3+} ions. Therefore, for the sake of simplicity, non-stoichiometry was not compensated for in the thermodynamic assessment of this study.

Habel et al. [4] showed experimentally a substitutional replacement of Ti^{4+} for V^{5+} in the rutile phase. Moreover, in our study on the Fe-V-O system in air, we assumed V dissolved substitutionally in the cation lattice of the hematite solid solution [1]. To remain consistent with previous modelling efforts and experimental findings, it was assumed that V dissolves substitutionally in the cation lattice. The model for the rutile solid solution is based on the second defect

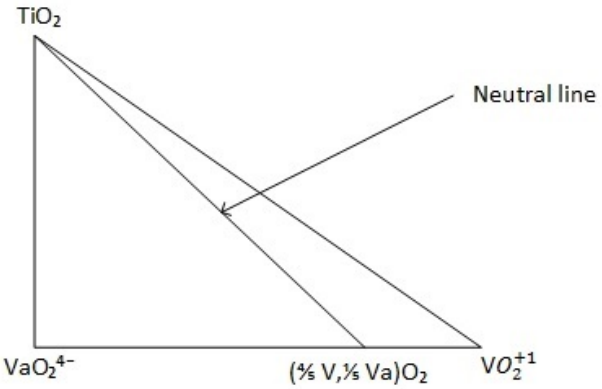

Figure 2: Schematic representation of end-member components and possible composition ranges on a neutral line of a rutile solid solution

model proposed by Habel et al. [4](see subsection 2.2). The model is represented by a mixture of V^{5+}, Ti^{4+} ions and vacancies on cation sites and oxygen being the only anion, in the second sub-lattice. Vacancies are introduced into the cation sub-lattice for charge neutrality. It has the chemical formula $(V^{5+},Ti^{4+},Va)(O)_2$, with charged end-member species used as model representatives, hence the excess term in Equation 13 is set to zero. A graphical illustration of the solution model is accomplished with a triangle plane with a neutral line (see Figure 2). The apexes of the triangle in Figure 2 each represent an end-member and each have the following chemical formulas: $Ti^{4+}O_2^{2-}, V^{5+}O_2^{2-}[+1]$ and $VaO_2^{2-}[-4]$. The molar Gibbs energy of rutile solid solution is expressed as follows:

$$\begin{aligned} G_{Rut} &= X_{Ti^{4+}}X_{O^{2-}}G^{\circ}_{Ti^{4+}:O^{2-}} + X_{V^{5+}}X_{O^{2-}}G^{\circ}_{V^{5+}:O^{2-}} + X_{Va}X_{O^{2-}}G^{\circ}_{Va:O^{2-}} \\ &+RT(X_{Ti^{4+}}lnX_{Ti^{4+}} + X_{V^{5+}}lnX_{V^{5+}} + X_{Va}lnX_{Va}) + 2RT(X_{O^{2-}}lnX_{O^{2-}}) + G_E \end{aligned} \tag{15}$$

However, two end-member compounds in the rutile solid solution are electrically charged and cannot physically exist. A compound exist on the rutile solid solution neutral line and this compound has the chemical formula $(\frac{4}{5}V,\frac{1}{5}Va)O_2$. It corresponds to 2/5 mole of V_2O_5(s), which again has a rutile-related structure. Therefore, the neutral specie, $(\frac{4}{5}V,\frac{1}{5}Va)O_2$ is a combination of the two electrically charged compounds and can be expressed as follows:

$$2/5G^{\circ}_{V_2O_5(s)-Rut} = \frac{4}{5}G^{\circ}_{V^{5+}:O^{2-}} + \frac{1}{5}G^{\circ}_{Va:O^{2-}} + RT\left(\frac{4}{5}ln\frac{4}{5} + \frac{1}{5}ln\frac{1}{5}\right) \tag{16}$$

with, $G^{\circ}_{V_2O_5(s)-Rut} = G^{\circ}_{V_2O_5(s)} + A + BT$.

The third term in Equation 16 is an entropy of mixing contribution on the cation sub-lattice. A and B are parameters that were optimized. Furthermore, the end-members are derived, rearranged and expressed as follows:

$$G^{\circ}_{Va:O^{2-}Rut} = 0 \tag{17}$$

$$G^{\circ}_{V^{5+}:O^{2-}Rut} = \frac{1}{2}G^{\circ}_{Rut-V_2O_5} - \frac{1}{4}G^{\circ}_{Va:O^{2-}} - \frac{5}{2}RT\left(\frac{4}{5}ln\frac{4}{5} + \frac{1}{5}ln\frac{1}{5}\right) \tag{18}$$

$$G^{\circ}_{Ti^{4+}:O^{2-}} = G^{\circ}_{TiO2(s)} \tag{19}$$

The terms, $G^{\circ}_{Va:O^{2-}Rut}$ are a reference term for other systems and have been set to zero [43, 1]. The other term, $G^{\circ}_{V_2O_5(s)-Rut}$ was optimized with respect to its enthalpy of formation and standard entropy.

5. Sequence of Optimization

The principle of data fitting and parameter optimization is based on a least-squares method. That is, an objective function is expressed as the difference between the calculated value of a given property and an experimental value of the same property. This difference is known as the residual. It is possible to acquire a set of optimized model parameters by minimizing the sum of the square of the residual over all measured points. The optimization was performed using the OPTISAGE tool in FactSage 7.0 which has the ability to consider all types of data simultaneously. The guidelines set by Lukas et al. [44] were closely followed in this assessment.

In the first step of optimization, the quasichemical temperature dependent parameters in Equation 12 were optimized to obtain a reasonable fit of the liquidus curve. The initial values of these parameters were set to zero, assuming ideal behaviour of the binary pairs, $Ti^{4+} - V_2O_3^{4+}$ and $Ti^{3+} - V_2O_3^{4+}$. Moreover, at this step of optimization, the solid solution, rutile, was modelled as pure TiO_2(s). Thereafter, the enthalpy of formation and standard entropy of $G^0_{V_2O_5(s)-Rut}$ from the rutile solid solution were optimized. $\Delta g_{Ti^{4+}-V_2O_3^{4+}}$ and $G^0_{V_2O_5(s)-Rut}$ were simultaneously optimized in the final step of optimization by considering experimental measurements from this study and the eutectic measurements (heating value) from Habel et al. [4]. The eutectic temperature of Solacolu and Zaharescu [2] was not considered, because in their work only a melt projection is presented, which in turn indicated a eutectic reaction in the V_2O_5-rich regime.

6. Results

6.1. Phase characterization and quantification

The polished and coated samples were analysed with EPMA and SEM-EDS. However, EPMA has been widely accepted as an analytical tool for high accuracy and precision quantification of liquid oxide phases [45]. Therefore, EPMA is also preferred in this study because of its ability to quantify oxygen concentration in phases more accurately.

To confirm sample homogeneity, at least ten points of each phase were analysed to calculate a set of standard deviations for each element. Only results from EPMA are shown in Table 4, however EDS results did not compare well to EPMA results, because it was noted that X-ray emission peaks of V and Ti overlapped. Oxygen concentration was calculated on the basis of stoichiometry (St.) by assuming V is in the 5+ and Ti in the 4+ oxidation state. The standard deviation (σ) of each element is shown in the table next to its mean concentration. Furthermore, the raw data in Table 4 were converted to mole % and normalized.

Table 4: Summary of raw data of the quenched samples analysed using EPMA in weight %.

	Molten Phase						Rutile solid solution					
Temperature °C	Ti	Ti (σ)	V	V (σ)	O (Stoichiometry)	Total	Ti	Ti (σ)	V	V (σ)	O (Stoichiometry)	Total
700	0.93	0.10	58.02	0.68	46.18	105.13	53.13	1.73	5.96	1.01	40.19	99.27
750	1.67	0.69	56.86	0.82	45.77	104.30	53.27	1.35	6.37	1.28	40.62	100.26
800	1.76	0.67	56.78	0.55	45.76	104.29	54.18	1.70	6.45	0.91	41.28	101.91
850	1.99	0.52	56.79	0.51	45.93	104.71	53.80	1.33	6.91	0.70	41.39	102.11
900	2.10	0.22	56.33	0.33	45.64	104.07	54.05	1.40	7.84	0.40	42.29	104.18
950	2.16	0.22	56.01	0.39	45.44	103.60	53.96	0.86	6.56	0.75	41.22	101.74
1000	2.35	0.19	57.11	0.89	46.42	105.88	51.71	0.62	9.23	0.17	41.81	102.75
1050	3.08	0.22	54.59	0.07	44.92	102.59	51.48	0.14	12.44	0.04	41.83	105.75
1100	3.16	0.28	55.35	0.72	45.58	104.09	45.06	0.57	15.14	0.69	42.01	102.20
1150	3.55	0.19	56.11	0.69	46.43	106.08	45.06	0.14	15.14	0.69	42.01	102.20
1200	3.49	0.42	55.25	0.84	45.72	104.46	46.81	0.33	13.44	0.23	41.85	102.09
1250	3.85	0.28	54.40	0.58	45.29	103.54	46.86	0.90	14.03	0.55	42.34	103.23
1300	3.84	0.32	55.25	0.94	45.95	105.04	45.44	1.06	15.43	0.21	42.49	103.37
1350	4.46	0.28	54.28	0.97	45.60	104.33	45.63	0.50	15.79	0.31	42.91	104.33
1400	4.67	0.32	54.53	1.04	45.94	105.15	45.63	0.57	15.57	0.26	42.73	103.93
1450	5.12	0.12	54.54	0.66	46.25	105.90	46.40	0.04	14.72	0.13	42.58	103.70
1500	5.18	0.19	53.88	0.49	45.76	104.82	46.85	0.64	14.49	0.23	42.70	104.05

All analysed samples had two phases, rutile solid solution and slag. Micrographs of samples captured from the SEM back scattered detector are shown in Figure 3. For the samples quenched at 800, 1000 and 1200 °C a homogeneous glassy slag phase surrounded by light grey TiO_2 crystals are observed. Less than 2.7 mole % Ti had dissolved in the slag phase, in contrast to a V solubility of more than 7.8 mole. % in the rutile solid phase at 1400 °C.

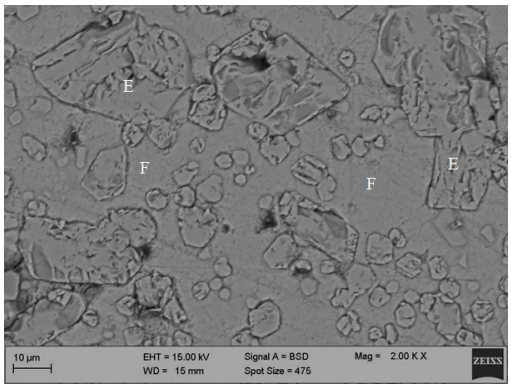

(a) 800 °C

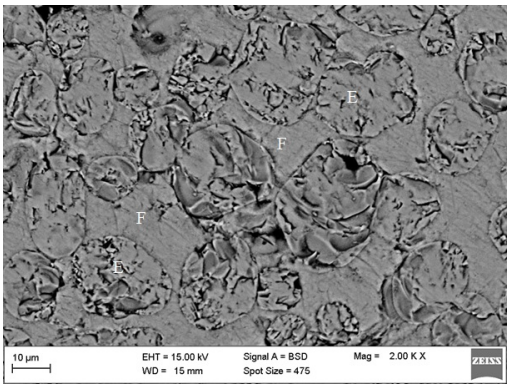

(b) 1000 °C

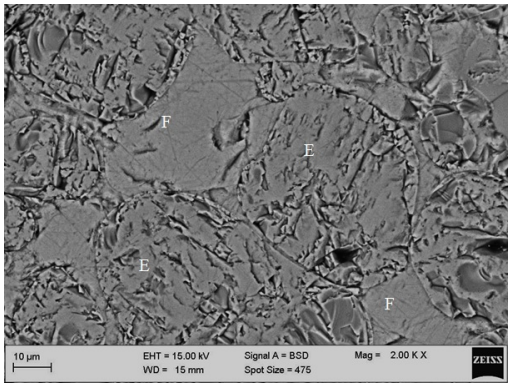

(c) 1200 °C

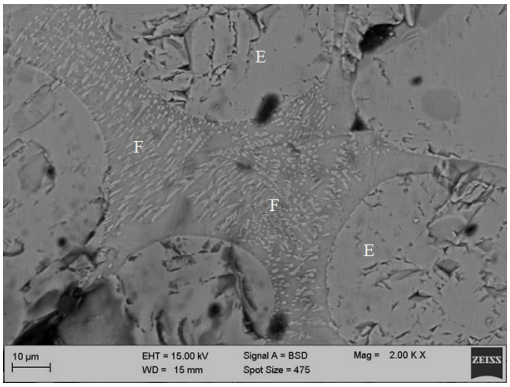

(d) 1500 °C

Figure 3: BSE micro-images of quenched samples: light crystals in (a), (b), (c) and (d) are rutile solid solution (E) and non-crystalline dark glassy phase is molten slag (F). Light crystals embedded in the molten slag in (d) are precipitate from quenching.

These findings indicate that the calculated $V_2O_5-TiO_2$ phase diagram from Yang et al. [7] were not entirely accurate owing to the shortage of experimental data on this system. Moreover, the calculated phase diagram from Yang et al. [7] grossly over-estimated the Ti solubility in the slag and under-estimated the V solubility in the rutile phase.

Some precipitates had formed in the slag phase for the sample quenched at 1500 °C. Sample size and quenching medium did not reduce precipitation in the slag phase. Furthermore, average composition between precipitates and glassy phase was calculated, utilizing a larger probe spot size and considering at least 15 areas in the slag phase. With this approach, a standard deviation below 1 % was calculated for samples quenched at 1500 °C.

6.2. Thermodynamic Calculations

Based on all experimental data from Habel et al. [4] and this study, the optimized model parameters for all phases in the Ti-V-O system in air are presented in Table 5. With these parameters, phase equilibria and invariant properties were calculated and compared with available literature data (where available).

A phase diagram, calculated from optimized parameters is shown in Figure 4. All superimposed experimental data on the diagram were considered during the optimization sequence. The V_2O_5-TiO_2 phase diagram data obtained from the thermodynamic assessment of Yang et al. [7] were mostly extrapolated from model parameters and were not considered in the assessment of this study.

The low solubility of Ti in the slag was reproduced with the MQM. The parameters $\Delta g^{\circ}_{Ti^{4+}-V_2O_3^{4+}}$ and $g^{01}_{\mathrm{Ti}^{4+}-\mathrm{V_2O_3^{4+}}}$ of Equation 12 were optimized and each had one temperature-independent coefficient. The $g^{01}_{\mathrm{Ti}^{4+}-\mathrm{V_2O_3^{4+}}}$ was found to have a negligible influence at low Ti solubility and may only become plausible and significant at a higher temperatures where Ti solubility is expected to increase. Nevertheless, $g^{10}_{\mathrm{Ti}^{4+}-\mathrm{V_2O_3^{4+}}}$ had been optimized after all other parameters

Table 5: Optimized parameters of solutions in the Ti-V-O system in air.

Liquid: TiO_2-Ti_2O_3-V_2O_5
TiO_2-Ti_2O_3 binary parameters Taken from the study of [35] V_2O_5-TiO_2 binary parameters $Z_{Ti^{4+}} = Z_{V_2O_3^{4+}} = 2.7548$ [11], $Z_{Ti^{3+}} = 2.0661$ [11] $g^{10}_{Ti^{4+}-V_2O_3^{4+}} = -56303.2$ $\Delta g^{\circ}_{Ti^{4+}-V_2O_3^{4+}} = 45402.4$ $g^{10}_{Ti^{4+}-V_2O_3^{4+}} = -33.5T$
Rutile Solid Solution $G^{\circ}_{V_2O_5(s)-Rut} = G^{\circ}_{V_2O_5(s)} + 195562 - 76.7190T - 20.8017T$ for MQM from 298 K to 1773 K

were optimized to reproduce the melting point of pure rutile. Without this parameter, unrealistic solutions were obtained at some temperatures and compositions between 1500 °C and the melting point of pure rutile. It was found that a temperature-dependent coefficient was more successful for reproducing the melting point of pure rutile. Moreover, the parameter did not significantly compromise the reproduced experimental results.

The rutile solid solution was reproduced successfully by adjustments to the enthalpy of formation and standard entropy of $G^{\circ}_{V_2O_5(s)}$. The adjusted value is shown separately to the derived value from the enthalpy of mixing. The eutectic temperature of the molten phase, rutile solid solution and V_2O_5(s) was calculated at 662 °C and at a $\frac{Ti}{(Ti+V)}$ mole ratio of 1.9 %. These values compared well with the thermal arrest upon heating, which was estimated by Habel et al. [4] to be about 670 °C and at a $\frac{Ti}{(Ti+V)}$ mole ratio of 2.6 %. The calculated eutectic temperature and composition also compared well toYang et al. [7] who calculated the eutectic temperature at 675 °C and at a $\frac{Ti}{(Ti+V)}$ mole ratio of 2.6 %.

7. Conclusions

The liquidus and solidus compositions on the Ti-V-O system in air were experimentally determined and analysed with SEM-EDS and EPMA. The liquid phase had a Ti concentration lower than 3 mole % within the entire investigated temperature range and coexisted with a rutile solid solution. The rutile solid solution had dissolved a maximum of 7.8 mole % V at 1400 °C and this phenomena has not been reported in any previous investigation.

A set of self-consistent thermodynamic parameters was achieved on the basis of the optimization considering data from present experiments and eutectic data from literature. A calculated phase diagram was provided, and the modified quasichemical model reproduced the experimental phase diagram data successfully. In addition, the phase diagram covers all areas between 1500 °C and the melting point of pure rutile, hence reasonable phase diagram can be estimated in areas not covered by experimental measurements. The rutile solid solution was well described with the compound energy formalism.

Future work can focus on acquiring liquidus and solidus data above 1500 °C; however other thermodynamic data such as enthalpy of mixing for liquid and activities of constituents of the liquid will be more valuable for an accurate description of the liquid phase in a similar temperature range as in this study. It is also our recommendation that a better understanding be gained of the defect models proposed and subsequently used to model the rutile solid solution.

8. Acknowledgements

This work was supported financially by the Glencore Chair in Pyrometallurgical Modelling at the University of Pretoria. We would also like to give gratitude to Prof Pekka Taskinen at Aalto University, School of chemical

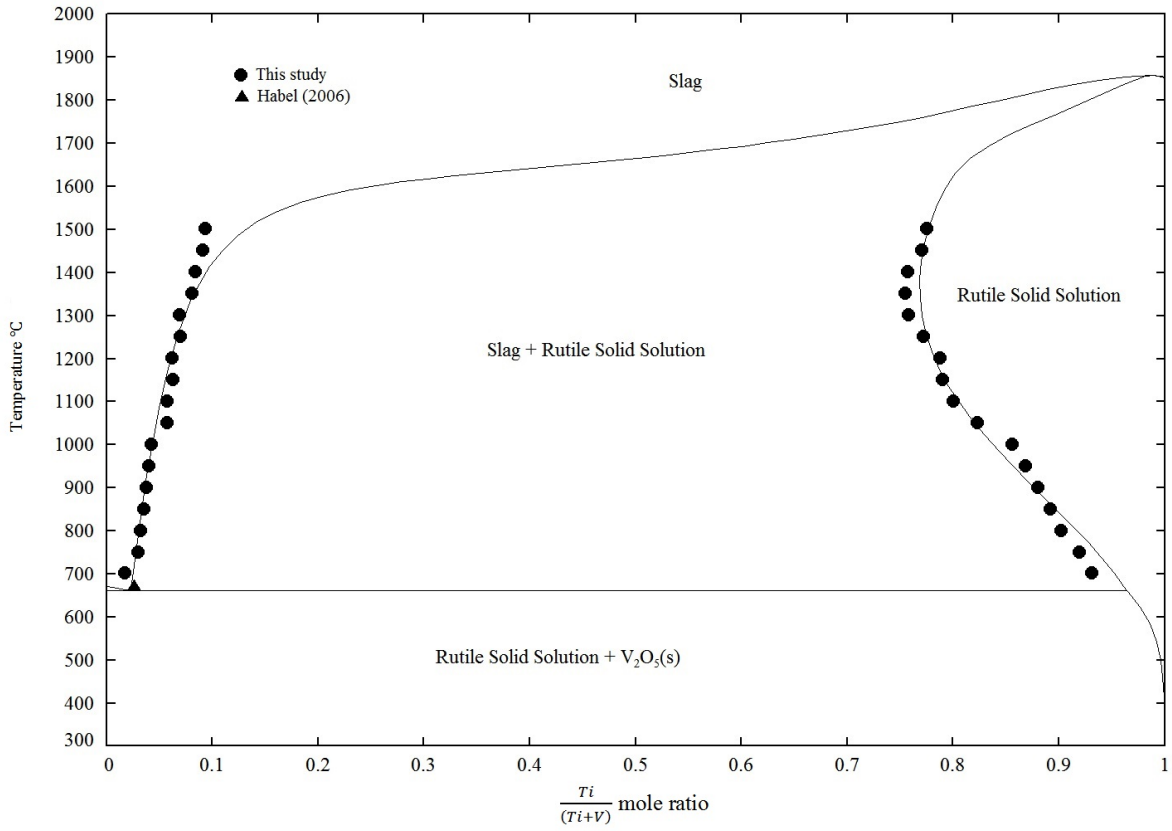

Figure 4: Equilibrium phase diagram of the Ti-V-O system in air compared with the present experimental works.

Engineering for lending their facilities to carry out experimental work. The authors of this work would further like to thank Dr Christian Reinke at the University of Johannesburg for his assistance and cooperation with EPMA work.

A. Supplementary information

The raw data required to reproduce these findings are available to download from [https://data.mendeley.com/submissions/evise/edit/gpy95rhz5j?submission_id=S0364-5916(18)30126-3&token=68458eac-2e97-4cbd-ae4a-a47eb70b4b72]. The processed data required to reproduce these findings are available to download from [https://data.mendeley.com/submissions/evise/edit/gpy95rhz5j?submission_id=S0364-5916(18)30126-3&token=68458eac-2e97-4cbd-ae4a-a47eb70b4b72].

References

[1] W. Malan, G. Akdogan, P. Taskinen, J. Hamuyuni, Phase equilibria and thermodynamic evaluation of Fe-V-O system in air, CALPHAD: Computer Coupling of Phase Diagrams and Thermochemistry 63 (2018) 12–23, URL https://doi.org/10.1016/j.calphad.2018.08.003.

[2] S. Solacolu, M. Zaharescu, Rev. Roum. Chim. 17 (1972) 1715–1724.

[3] A. A. Fotiev, L. L. Surat, A. I. Tret'yakov, Compatibility relations in the $Fe_2O_3-TiO_2-V_2O_5$, $Cr_2O_3-TiO_2-V_2O_5$ and $Al_2O_3-TiO_2-V_2O_5$ systems, Russian journal of inorganic chemistry 26 (5) (1981) 1377–1382.

[4] D. Habel, J. Stelzer, E. Feike, C. Schroder, A. Hosch, C. Hess, A. Knop-Gericke, J. Caro, H. Schuber, Phase development in the catalytic system V_2O_5/TiO_2 under oxidiising conditions, Journal of European Ceramic Society 26 (2006) 3287–3294, URL http://dx.doi.org/10.1016/j.jeurceramsoc.2005.09.108.

[5] D. Habel, O. Goerke, M. Tovar, E. Kondratenko, H. Schubert, Phase relations in the system TiO_2-V_2OxunderOxidizingandreducingconditions, Journal of Phase Equilibria and Diffusion 29 (6) (2008) 482–487, URL http://dx.doi.org/110.1007/s11669-008-9391-z.

[6] M. Enomoto, The O-Ti-V System (Oxygen-Titanium-Vanadium), J. Phase Equilib. 17 (6) (1996) 539–545, URL https://doi.org/10.1007/BF02666001.

[7] Y. Yang, H. Mao, H. Chen, M. Selleby, An assessment of the Ti-V-O system, Journal of Alloys and Compounds 722 (2017) 365–374, URL https://doi.org/10.1016/j.jallcom.2017.05.326.

[8] Z. Hiroi, H. Hayamizu, T. Yoshida, Y. Muraoka, Y. Okamoto, J. Yamaura, Y. Ueda, Spinodal Decomposition in the TiO_2-VO_2 System, Journal of Alloys and Compounds 25 (11) (2013) 2202–2210, URL https://DOI:10.1021/cm400236p.

[9] A. Vejux, P. Courtine, Interfacial reactions between V_2O_5 and TiO_2 (Anatase): Role of the structural properties, Journal of Solid State chemistry 23 (1) (1978) 93–103, URL http://dx.doi.org/10.1016/0022-4596(78)90055-5.

[10] G. Bond, A. J. Sarkany, G. Parfitt, The Vanadium Pentoxide-Titanium Dioxide System: Structural investigation and actvity for the oxidation of Butadiene, Journal of Catalysis 57 (4) (1979) 476–493, URL http://dx.doi.org/10.1016/0021-9517(79)90013-7.

[11] C. Bale, E.Belisle, P. Chartand, S. Decterov, G. Eriksson, K. Hack, I. Jung, Y. Kang, J. Melancon, A. Pelton, C. Robelin, S. Petersen, FactSage thermochemical software and databases, 2010-2016, CALPHAD: Computer Coupling of Phase Diagrams and Thermochemistry 54 (2) (2016) 35–53, URL https://doi.org/10.1016/j.calphad.2008.09.009.

[12] B. G. Golovkin, V. L. Volkov, V. D. Skobeleva, Subsolidus regions in the $CaO-TiO_2-V_2O_5$ system, Russian journal of inorganic chemistry 34 (9) (1989) 1337–1339.

[13] M. Chase, J. Curnutt, H. Prophet, R. Mcdonald, JANAF thermochemical tables supplement, Journal of physical chemistry data 4, URL http://dx.doi.org/10.1007/BF02873201.

[14] J. Murray, H. Wriedt, The O-Ti (Oxygen-Titanium) system, Bulletin of Alloy phase diagrams 8 (2) (1987) 148–165, URL http://dx.doi.org/10.1007/BF02873201.

[15] M. Cancarevic, M. Zinkevich, F. Aldinger, Thermodynamic description of the Ti-O system using the associate model for the liquid phase, CALPHAD: Computer Coupling of Phase Diagrams and Thermochemistry 31 (2007) 330–342, URL http://dx.doi.org/10.1016/j.calphad.2007.01.009.

[16] D. Hanaor, C. Sorrel, Review of the anatase to rutile phase transformation, J. Mater. Sci. 46 (2009) 855–874, URL https://doi.org/10.1007/s10853-010-5113-0.

[17] C. Alcock, C. Ji, Vanadium-oxygen system. A Review, High Temperature - High Pressures 22 (2) (1990) 139 – 147.

[18] H. Wriedt, The O-V Oxygen - Vanadium system, Bulletin of Alloy Phase Diagrams 10 (3) (1989) 271 – 277, URL http://dx.doi.org/10.1007/BF02877512.

[19] Y. Kang, Critical evaluation and thermodynamic optimization of the VO - $VO_2 \cdot 5$, Journal of the European Ceramic Society 32 (2012) 3187 – 3198, URL http://dx.doi.org/10.1016/j.jeurceramsoc.2012.04.45.

[20] Y. Yang, H. Mao, M. Selleby, Thermodynamic assessment of the V-O system, CALPHAD: Computer Coupling of Phase Diagrams and Thermochemistry 51 (2015) 144–160, URL http://dx.doi.org/10.1016/j.calphad.2015.08.003.

[21] R. Robert, CRC Handbook of Chemistry and Physics, vol. 62, Boca Raton, FL: CRC Press, Cambridge, UK, URL ISBN0-8493-0462-8, 1981.

[22] C. Merlet, An Accurate Computer Correction Program for Quantitative Electron Probe Microanalysis, Mikrochim.Acta 114/115 (1994) 363–376.

[23] M. Koretsky, Engineering and chemical thermodynamics, vol. 1, John Wiley and Sons, Inc., 111 River Street, Hoboken, NJ 07030, 2004.

[24] A. Pelton, M. Blander, Thermodynamic Analysis of Ordered Liquid Solutions by a Modified Quasi-Chemical Approach - Application to Silicate Slags, Met. Trans. B 17B (1986) 805–815, URL https://doi.org/10.1007/BF02657144.

[25] A. Pelton, M. Blander, Thermodynamic Analysis of Binary-Liquid Silicates and Prediction of Ternary Solution Properties by Modified Quasi-Chemical Equations, Geochim. Cosmochim. Acta 51 (1987) 85–95.

[26] Y. Kawakita, H. Nakashima, S. Yoshioka, S. Takeda, K.Maruyama, M. Inui, K. Tamura, Local structures of liquid and vitreous V_2O_5 and P_2O_5, Journal of Physics and Chemistry of Solids 60 (1999) 1483 – 1486, URL http://dx.doi.org/S0022-3697(99)00148-1.

[27] S. Hawakawa, T. Yoko, IR and NMR structural studies on lead vanadate glasses, Journal of non-crystalline solids 183 (1995) 73–84.

[28] P. Hudon, I. Jung, Critical evaluation and thermodynamic optimization of the $CaO-P_2O_5$ system, Metallurgical and Materials Transactions B 46 (B) (2014) 494–522.

[29] M. Rahman, P.Hudon, I. Jung, A coupled experimental study and thermodynamic modelling of the $SiO_2-P_2O_5$ system, Metallurgical and Materials Transactions B 44 (B) (2013) 837–852.

[30] C. Bale, P.Chartrand, S. Degterov, G.Eriksson, K.Hack, R. Mahfoud, J. Melancon, A. Pelton, S.Petersen, FactSage thermochemical software and databases, CALPHAD: Computer Coupling of Phase Diagrams and Thermochemistry 26 (2) (2002) 189–228, URL http://dx.doi.org/10.1016/S0364-5916(02)00035-4.

[31] H. Suito, D. Gaskell, The thermodynamics of melts in the system $VO_2-V_2O_5$, Metallurgical and Materials Transactions B 2 (12) (1971) 3299–3303, URL https://doi.org/10.1007/BF02811610.

[32] W. Xie, N.Wang, Z. Qiao, Z. Cao, Thermodynamic assessment of the PbO - V_2O_5 system, CALPHAD: Computer Coupling of Phase Diagrams and Thermochemistry URL http://dx.doi.org/10.1016/j.calphad.2016.04.005.

[33] Z. Cao, N. Wang, W. Xie, Z. Qiao, I. Jung, Critical evaluation and thermodynamic assessment of the $MgO-V_2O_5$ and $CaO-V_2O_5$ systems in air, CALPHAD: Computer Coupling of Phase Diagrams and Thermochemistry 56 (2017) 72–79, URL http://dx.doi.org/10.1016/j.calphad.2016.12.001.

[34] G. Eriksson, A. Pelton, Critical evaluation and optimization of the thermodynamic properties and phase diagrams of the $MnO-TiO_2$, $MgO-TiO_2$, $FeO-TiO_2$, $Ti_2O_3-TiO_2$, Na_2O-TiO_2 and K_2O-TiO_2 systems, Metallurgical Transactions B 24 (B) (1993) 795–805, URL http://dx.doi.org/10.1007/BF02663140.

[35] Y. Kang, I. Jung, H. Lee, Critical evaluation and optimization of the $MnO-TiO_2-Ti_2O_3$ system, CALPHAD: Computer Coupling of Phase Diagrams and Thermochemistry 30 (2006) 235–247, URL http://dx.doi.org/10.1016/j.calphad.2006.05.001.

[36] G. Eriksson, A. Pelton, G. Eriksson, S. A. Degterov, C. Robelin, Y. Dessurrault, The Modified Quasichemical Model I-Binary Solutions, Metallurgical and Materials Transactions B 31 (B) (2000) 651–659, URL http://dx.doi.org/10.1007/s11663-000-0103-2.

[37] N.Wang, Critical evaluation and thermodynamic assessment of the $CaO-MgO-V_2O_5$ system, M.sc. thesis, University of Science and Technology, Beijing, 2015.

[38] V. Protstakova, J.Chen, E.Jak, S. Decterov, Experimental investigation and thermodynamic modelling of the $(NiO+CaO+SiO_2)$ and $(NiO+CaO+MgO+SiO_2)$, J. Chem. Thermodynamics 86 (B) (2015) 130–142, URL http://dx.doi.org/10.1016/j.jct.2015.01.017.

[39] A. Pelton, A general "Geometric" thermodynamic model for multicomponent solutions, CALPHAD: Computer Coupling of Phase Diagrams and Thermochemistry 25 (2) (2001) 319–328, URL https://doi.org/10.1016/S0364-5916(01)00052-9.

[40] I. Jung, S. Deceterov, A. Pelton, Critical thermodynamic optimization of the Fe-Mg-O system, Journal of Physics and Chemistry of Solids 65 (1) (2004) 1683–1695, URL http://dx.doi.org/10.1016/j.jpcs.2004.04.005.

[41] W. Zhang, M. Chen, Thermodynamic modelling of the Co-Fe-O system, CALPHAD: Computer Coupling of Phase Diagrams and Thermochemistry 41 (1) (2013) 76–88, URL http://dx.doi.org/10.1016/j.calphad.2013.02.002.

[42] V. Prostakova, J.Cheng, E.Jak, S. Decterov, Experimental investigation and thermodynamic modeling of the $NiO-CaO-SiO_2$, NiO-CaO-SiO2 and $NiO-CaO-MgO-SiO_2$ systems, Journal of chemical thermodyanamics 86 (2015) 130–142, URL http://dx.doi.org/10.1016/j.jct.2015.01.017.

[43] T. Zieniert, O. Fabrischnaya, Thermodynamic assessment and experiments in the system $MgO-Al_2O_3$, CALPHAD: Computer Coupling of Phase Diagrams and Thermochemistry 40 (2015) 1–9, URL http://dx.doi.org/10.1016/j.calphad.2012.10.001.

[44] H. Lukas, S. Fries, B. Sundman, Computational thermodynamics, the Calphad method, Cambridge University press, Cambridge, UK, 2007.

[45] D. Newbury, N. Ritchie, Performing elemental microanalysis with high accuracy and high precision by scanning electron microscopy/silicon dirft detector energy-dispersive X-ray spectrometry, Journal of Material Science 50 (2015) 493–518, URL http://dx.doi.org/10.1007/s10853-014-8685-2.